

Morphology of Hydrated As-Cast Nafion Revealed through Cryo Electron Tomography

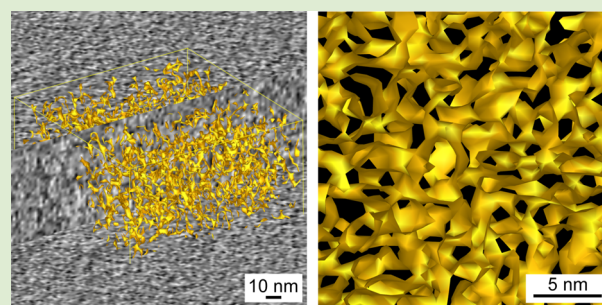
Frances I. Allen,^{*,†,‡} Luis R. Comolli,^{§,□} Ahmet Kusoglu,^{||} Miguel A. Modestino,^{⊥,○} Andrew M. Minor,^{†,‡} and Adam Z. Weber^{||}

[†]Department of Materials Science and Engineering and [⊥]Department of Chemical and Biomolecular Engineering, University of California, Berkeley, California 94720, United States

[‡]National Center for Electron Microscopy, Molecular Foundry, [§]Life Sciences Division, and ^{||}Environmental Energy Technologies Division, Lawrence Berkeley National Laboratory, Berkeley, California 94720, United States

Supporting Information

ABSTRACT: Nafion is an ion-containing random copolymer used as a solid electrolyte in many electrochemical applications thanks to its remarkable ionic conductivity and mechanical stability. Understanding the mechanism of ion transport in Nafion, which depends strongly on hydration, therefore requires a complete picture of its morphology in dry and hydrated form. Here we report on a nanoscale study of dry versus hydrated as-cast 100 nm Nafion membranes using analytical transmission electron microscopy (TEM) and cryogenic TEM tomography, respectively. For the dry membrane, spherical clusters ~3.5 nm in diameter corresponding to the hydrophilic sulfonic-acid-containing phase are identified. In contrast, cryo TEM tomography of the hydrated membrane reveals an interconnected channel-type network, with a domain spacing of ~5 nm, and presents the first nanoscale 3D views of the internal structure of hydrated Nafion obtained by a direct-imaging approach.



Cryo TEM 3D reconstructions of hydrated Nafion

The development of Nafion by DuPont in the 1960s marked the dawn of a new class of synthetic polymers now known as ionomers.¹ Constituting a tetrafluoroethylene (Teflon) backbone and side chains terminated by sulfonic-acid groups (see Figure 1), Nafion combines the mechanical

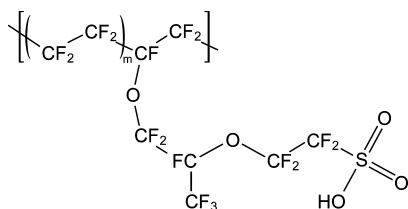


Figure 1. Chemical structure of Nafion (EW 1100), $m = 6.5$.¹

strength and chemical resistance of the former, with exceptional ion-transport properties imparted by the latter. To this day, Nafion continues to find application in a range of technologies that rely on this unique combination of properties. Of great interest is the use of Nafion and other related perfluorosulfonic-acid ionomers in proton exchange membrane (PEM) fuel cells, a viable candidate for clean-energy transportation needs.^{2–4}

Obtaining a complete picture of the morphology of Nafion is crucial for a mechanistic understanding of ion transport through the material. Yet despite Nafion's long-term and widespread use, its morphology remains controversial.^{1,5–9}

Attributes that are well-established include semicrystallinity of the Teflon phase and microphase separation of the random copolymer into a disordered arrangement of hydrophobic (Teflon) and hydrophilic (sulfonic acid) domains. Upon hydration, Nafion membranes swell forming nanoscale hydrophilic water clusters, as indicated by the characteristic “ionomer peak” observed in small-angle X-ray/neutron scattering (SAXS/SANS) experiments. In this phase-separated network of water-filled domains, transport occurs depending on the size, shape, and connectivity of the domains. In the fully hydrated state, Nafion swells up to ~50% by volume accommodating more than 20 water molecules per sulfonic-acid group without losing stability. However, the exact nature of the phase-separated structure is still disputed and a range of morphological descriptions has been proposed,^{1,7} including a network of interconnected nanoscale spherical water clusters,^{5,6} parallel cylindrical water nanochannels,⁸ a ribbon-like structure of polymer separated by water molecules,¹⁰ a bicontinuous network of hydrophilic domains,¹¹ and a locally flat, layered structure of water domains.^{9,12}

In addition to the highly disordered and also dynamic nature of the structure of Nafion, further difficulties in assigning a definitive morphology arise as a result of the varying solubilities

Received: September 22, 2014

Accepted: December 3, 2014

Published: December 20, 2014

and crystallinities of Nafion's various derivatives, with electrostatic interactions adding to the complexity of the problem. Casting conditions, thermal history, counterion type, as well as thickness when confined to thin films, also influence the morphology of the phase-separated domains,^{5,6,13–15} yet certainly the most important variable is the degree of hydration.^{1,6,16,17}

Structural studies have mainly used X-ray and neutron scattering results obtained in SAXS and SANS experiments.⁷ The analysis of this data relies on molecular or mesoscale models developed to generate theoretical scattering patterns to match the experimental results, and the interpretation can be complex since the patterns are typically comprised of only a couple of broad peaks,^{8,9,11} thereby making a unique interpretation difficult. For direct imaging of Nafion at the nanoscale, atomic force microscopy (AFM)^{18,19} and transmission electron microscopy (TEM),^{5,14,20–25} respectively, have been employed. While AFM can be performed on hydrated (i.e., ambient) Nafion samples with relative ease, it can only reveal surface topology. TEM, on the other hand, probes internal morphologies by generating 2D volume-projections, however, studies have mainly investigated dried samples (due to the instrument's high-vacuum requirements) and not without some controversy. TEM of hydrated materials is enabled using cryogenic techniques, yet few cryo TEM results for hydrated Nafion membranes have been reported^{24,26} and none using cryo TEM tomography, which can yield the 3D internal structure.

In this work, we compare the nanoscale morphology of dry and hydrated Nafion membranes by direct imaging using analytical TEM and cryo TEM tomography, respectively. Films are cast to a thickness of ~ 100 nm, thereby ensuring electron transparency. Experimental studies reported elsewhere including measurements of water uptake, swelling, conductivity, and scattering have shown that the phase separation of both annealed and unannealed 100 nm membranes approaches that of bulk membranes.^{14,15,27,28} In a set of baseline studies, we establish the identity and morphology of the hydrophobic and hydrophilic domains in dry as-cast 100 nm Nafion membranes, after which we proceed to the study of hydrated membranes, the main focus of this work. These samples are prepared and imaged adhering to the cryo TEM protocols developed in the biological imaging community, ensuring that the intact hydrated Nafion morphology is probed. Finally, the results of cryo TEM tomography studies are presented, revealing the 3D morphology of the hydrated Nafion membranes.

Figure 2a shows the phase separation observed for dry unstained 100 nm Nafion membranes by bright-field TEM. A random distribution of spherical domains (dark contrast) 3.5 ± 0.3 nm in diameter is found. Electron microscopy studies have often used heavy-element stains (e.g., RuO_4)²² or ion-exchange (e.g., Pb^+ , Cs^+)^{5,20,21} for contrast enhancement and identification of the ionic domains in Nafion, finding cluster diameters ranging from 3 to 10 nm. However, stains are known to generate artifacts and ion-exchange can cause swelling behavior. Crystallization of the heavy ions during electron-beam irradiation in the microscope has also been observed.²¹ We attribute the smaller cluster sizes measured in our work principally to the avoidance of heavy-element pretreatment procedures in our study. Using spectroscopic contrast to distinguish the phases in the Nafion membrane, Figure 2b shows chemical mapping results where energy-filtering TEM spectrum-imaging (EFTEM SI) has been applied

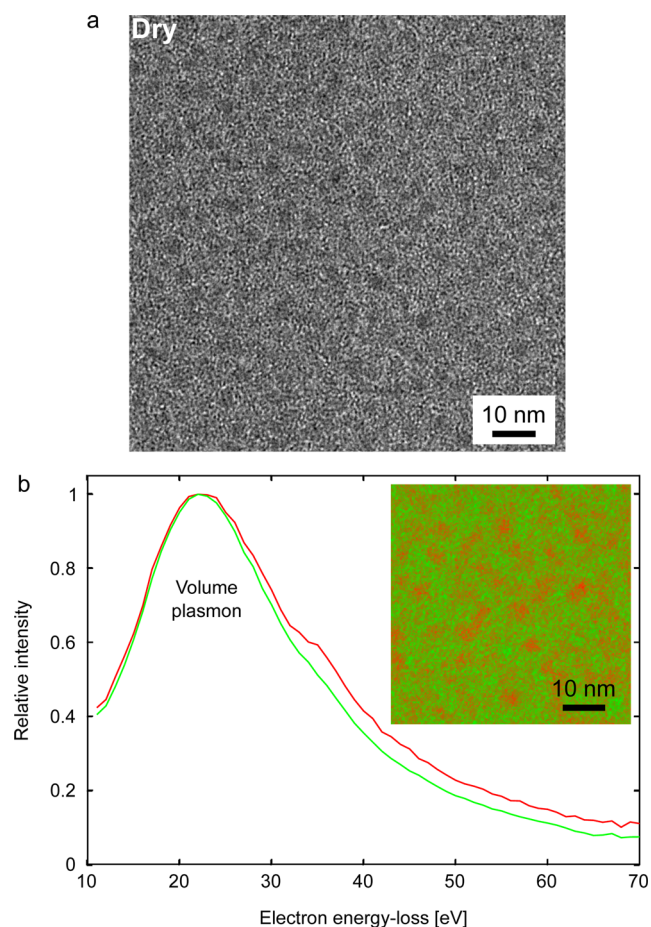


Figure 2. TEM imaging and EFTEM chemical mapping of a dry 100 nm Nafion membrane. (a) Bright-field TEM, (b) EFTEM SI results showing volume plasmons extracted for each phase, with composite chemical map for the clusters (red) and matrix (green), inset.

in the low electron energy-loss range to probe the morphology of the untreated dry Nafion membrane based on subtle differences in the volume plasmon resonances of the polymer phases.^{14,29,30} The distinct plasmon resonance spectra for the spherical domains and the matrix phase are shown in red and green, respectively, with the corresponding composite chemical map inset. The morphology revealed in the chemical map reflects that observed in the bright-field TEM images. We note that, for the cluster phase, a shoulder in the low-loss spectrum at ~ 35 eV is observed. This could be attributed to the core-shell $L_{2,3}$ transition in sodium, possibly introduced as an impurity during the sample preparation procedure.

To determine the identity of the two phases observed by TEM and EFTEM-based chemical mapping, elemental mapping of dry, untreated Nafion membranes has been performed with high sensitivity using X-ray energy-dispersive spectrometry (XEDS). In this technique, the electron beam is focused to a spot size of ~ 1 nm and scanned across the sample to generate an X-ray spectrum for each point in the scan. In Figure 3a, a high-angle annular dark-field (HAADF) scanning TEM (STEM) image is shown together with the corresponding XEDS elemental maps calculated based on the characteristic X-rays detected for (b) C, (c) F, (d) O, (e) S, and (f) Cu. In the HAADF STEM image, the cluster domain now forms the bright contrast. The composition of the hydrophobic CF_2 backbone versus the hydrophilic side groups of Nafion differs only in the

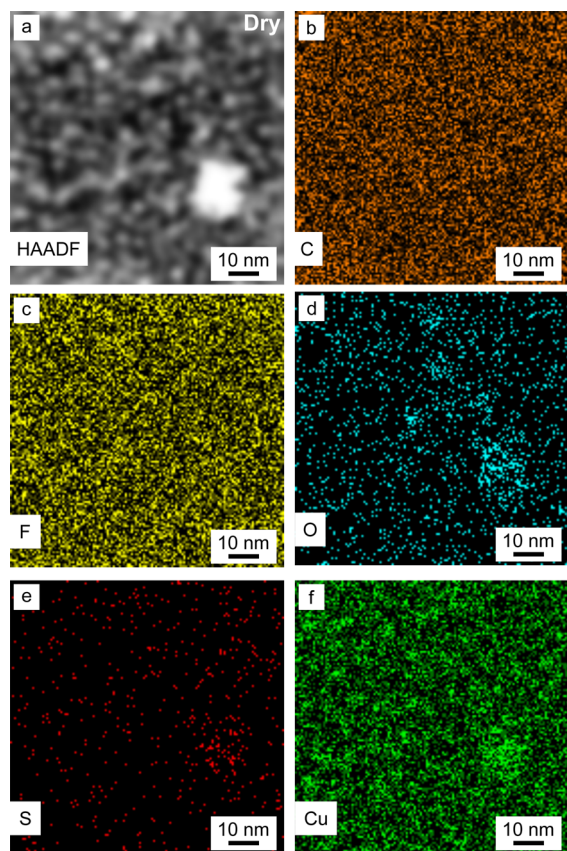


Figure 3. XEDS elemental mapping of a dry 100 nm Nafion membrane. (a) Reference HAADF STEM image; XEDS elemental maps for (b) C, (c) F, (d) O, (e) S, and (f) Cu.

presence of a relatively small fraction of O, S, and H atoms in the latter (see Figure 1), thus, considering that the mass density of the hydrophobic and hydrophilic domains in the phase-separated membrane must be very similar, the contrast observed in the TEM and STEM images of Figures 2a and 3a, respectively, is at first somewhat surprising. Recently, however, it has been shown that Cu ions diffuse into Nafion membranes prepared on Cu-mesh substrates.²⁴ In our work, Cu substrates were also used (a TEM standard); thus, in addition to the distributions of those elements native to Nafion, the distribution of Cu was also investigated. The distributions of C and F revealed in Figure 3 appear homogeneous, whereas the distributions of O, S, and Cu show enhanced concentrations in particular regions. In the lower right quadrant of the STEM image of Figure 3a, a large 15–20 nm agglomerated cluster is seen (such agglomerations were found across the entire sample) and the concentrations of O, S, and Cu are found to be higher in this region. There is also a correlation between the O, S, and Cu distributions and some of the smaller spherical domains in the STEM image (more obvious for brighter domains).

From the XEDS results we thus infer that the spherical clusters observed in the dry Nafion membranes correspond to the hydrophilic O- and S-containing domains in the polymer, and that Cu ions from the grid presumably ion-exchanged with protons on the sulfonic-acid groups. This likely occurs during transfer of the Nafion membranes to the grid substrates, which is carried out in water. The presence of Cu in the hydrophilic cluster regions of the membrane would increase the mass-

contrast of those regions, explaining the contrast observed in the TEM and STEM images. As a control, we also prepared Nafion membranes on nonstandard Cu-free substrates. TEM imaging of these membranes shows only faint clusters, that is, the contrast difference between the two phases is very small (see Figure S1). The results of supplementary studies of dry membranes demonstrating significant swelling behavior as a result of pretreatment by Fe-ion exchange are shown in Figure S2.

In Figure 4a, we present a bright-field cryo TEM image of an as-cast, frozen-hydrated 100 nm Nafion membrane with a

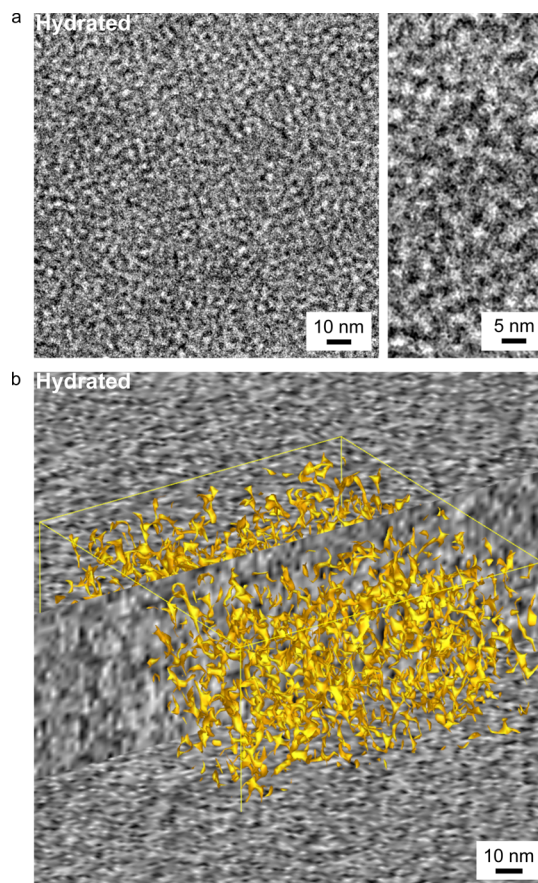


Figure 4. Cryo TEM of a frozen-hydrated, as-cast 100 nm Nafion membrane. (a) Bright-field cryo TEM (2D projection) with magnified region shown on the right, (b) cryo TEM 3D reconstruction with two perpendicular slices through the tomogram shown; yellow marks the spatial distribution of the central region of the dark (hydrophilic) phase using isosurface rendering. Noise reduction and contrast enhancement have been applied as described in the Supporting Information.

magnified region shown on the right. There is a striking difference between the morphology of the frozen-hydrated membrane and the morphology of the dry membrane shown in Figure 2a. Rather than a random distribution of spherical domains, a random interconnected channel-type morphology is revealed in the hydrated case. The width of the channels is measured at 2.5 ± 0.2 nm and the domain spacing (i.e., the center-to-center spacing between dark (or bright) channels) is 5.1 ± 0.5 nm. A combination of the low-dose imaging conditions, sample-thickness scattering effects, and phase mixing of the polymer itself likely gave rise to the distribution of values measured in each case. We note that focal series

measurements were performed in order to select appropriate defocus conditions that optimized phase contrast without sacrificing the spatial resolution required to resolve the domains (Figure S3). Dose series were also acquired to determine electron doses that ensure that the morphologies captured were not significantly altered by radiation damage effects (Figure S4).

Previous cryo TEM studies of hydrated Nafion have each yielded conflicting results and have not included 3D investigations by cryo TEM tomography.^{24,26} Here, Figure 4b presents the results of a 3D tomographic reconstruction obtained from a cryo TEM tilt series of the hydrated sample. All tomographic reconstructions were obtained using the programs Imod (<http://bio3d.colorado.edu/>) and Tomo3d (<https://sites.google.com/site/3demimageprocessing/tomo3d>).³¹ Two perpendicular slices through the reconstruction are shown, displaying vertical and horizontal cross sections through the membrane. Isosurface rendering (in yellow) is used to mark the 3D spatial distribution of the darker (hydrophilic) phase, highlighting only the central portion in this particular representation for viewing purposes. A magnified region of this reconstruction is shown in Figure S5. The 3D results indicate that the channel-type morphology observed in Figure 4a propagates continuously throughout the thickness of the membrane. Figure 5 shows isosurface rendering for a 3D

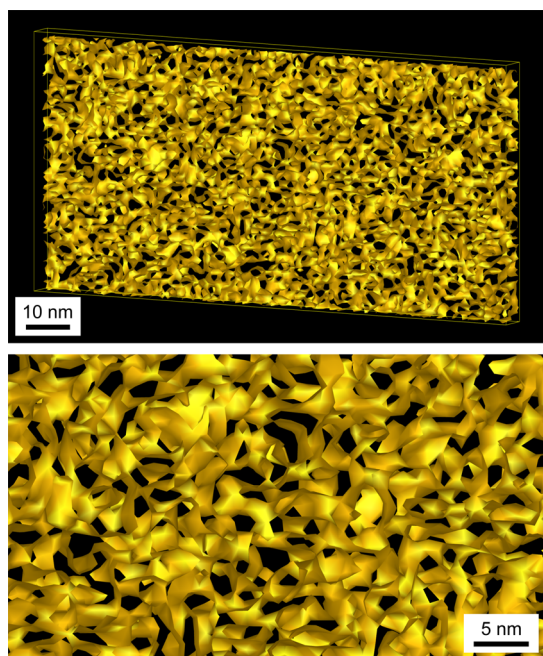


Figure 5. Isosurface-rendered 3D reconstruction of the frozen-hydrated as-cast Nafion membrane (low- and high-magnification views) highlighting the spatial distribution of the hydrophilic phase in yellow, which has a volume fraction of 0.55 as calculated from the 3D results; details in the Supporting Information.

volume slab of the reconstruction in which the entire volume of the hydrophilic phase is enclosed. It is found that the hydrophilic channels form a multibranching complex network and we also note that the channels are not uniformly cylindrical in shape.

Our results indicate that upon hydration the morphology of the Nafion membrane transforms from the isolated hydrophilic clusters of the dry state to a branched channel-type structure

that enables proton conductivity to occur. The random nanoscale channel-type 3D network of hydrated Nafion determined here for the first time by a direct-imaging approach essentially supports the phase-separated bicontinuous network morphologies obtained in a number of atomistic, molecular, and mesoscale simulations.^{11,25,32–34} The domain spacings of 5.1 ± 0.5 nm are in good agreement with those determined by SAXS. We have also performed SAXS measurements on Nafion membranes immersed in various concentrations of Cu-ion solutions and find that the domain spacings obtained from our cryo TEM data are consistent with the low Cu-concentration SAXS values (see Figure S6). Therefore, even though Cu ions from the TEM grid substrates are observed to accumulate in the hydrophilic phase (as shown for the dry membrane in Figure 3), the degree of ion exchange appears to be low enough not to significantly impact the domain spacings in the hydrated material. Interestingly, we find that an increase in the concentration of Cu available for ion exchange actually decreases the spacing of the hydrophilic domains, which we attribute to the divalent Cu ions binding the sulfonic-acid chains in the clusters more tightly than the protons they replace. It should be noted that the basic shape of the SAXS profiles is not affected by Cu concentration, indicating that the morphology causing the scattering remains similar regardless of Cu ion-exchange.

From the 3D data we are also able to compute volume fractions of the hydrophilic and hydrophobic phases using a gray-value thresholding approach (see Figure S7) to compare with theoretical values calculated from experimental membrane water-uptake and swelling data. For the dark channels in the hydrated membrane (i.e., the phase containing the hydrophilic component), an experimental volume fraction of 0.55 ± 0.02 is obtained, which is in good agreement with the theoretical volume fraction of 0.57 ± 0.10 calculated taking phase mixing into account (details in the Supporting Information). We also note that while it is well-known that the tetrafluoroethylene backbone of Nafion exhibits semicrystallinity, such crystallites were not observed in our TEM surveys. However, given that we investigated Nafion membranes cast to thin films without annealing, for which the degree of crystallinity is known to be suppressed,^{15,27} this result is not unexpected (see Figure S8 showing a grazing-incidence SAXS (GISAXS) line profile for 100 nm as-cast hydrated Nafion). Upon increasing the degree of crystallinity in the thin film by annealing, a decrease in the amount of water uptake would be expected, resulting in smaller domain spacings.

Finally, we have computed simulated SAXS profiles from the 3D cryo TEM reconstructions following a 3D Fourier transform and radial averaging approach.³⁵ Calculating for a 3D reconstruction thresholded at the midpoint gray value (corresponding to the volume fraction of the hydrophilic phase of 0.55, as in Figure 5), the small-angle upturn and broad ionomer peak characteristic of experimental SAXS profiles are reproduced. The simulated SAXS profile is presented in Figure S9 and validates the 3D cryo TEM reconstruction results obtained in this work. As expected the matrix peak is not observed, due to the suppression of crystallinity in our as-cast membranes.

In summary, two distinct nanoscale morphologies for dry versus hydrated Nafion membranes have been revealed by direct imaging using a range of advanced electron-microscopy techniques. The general consensus from TEM studies of dry Nafion has been a morphology comprising isolated nanoscale

ionic clusters. Our work supports this result and we have extended these studies using analytical TEM techniques to map and identify the hydrophilic and hydrophobic domains in the dry membrane. In Nafion's hydrated form, in which proton transport occurs, it is clear that connectivity between the domains must be present. Here we have used cryo TEM tomography to reveal the nanoscale 3D morphology of the hydrated membrane for the first time finding a random channel-type interconnected network. Cryo TEM tomography allowed us to obtain the 3D internal structure of hydrated Nafion directly, as opposed to having to rely on interpretations based on 2D volume-projections. Moreover, by preparing the hydrated membranes following rigorous cryo TEM protocol and employing low-dose cryo TEM tomography techniques, determination of the intact morphology with nanoscale resolution was achieved. With the 3D structure of hydrated as-cast Nafion thus revealed, future research can use refined structural models and structure/function relationships to understand the ion transport mechanisms in this material and facilitate the development of new ionomers with high ionic conductivities.

■ ASSOCIATED CONTENT

■ Supporting Information

Additional TEM results for dry membranes, cryo TEM dose and focal series, SAXS and GISAXS data, additional isosurface renderings, volume fraction calculations, simulated SAXS profiles, experimental methods, and data processing. This material is available free of charge via the Internet at <http://pubs.acs.org>.

■ AUTHOR INFORMATION

Corresponding Author

* E-mail: fiallen@lbl.gov.

Present Addresses

□Molecular Biology Consortium, Advanced Light Source Beamline 4.2.2, Lawrence Berkeley National Laboratory, Berkeley, CA 94720, U.S.A. (L.R.C.).

○School of Engineering, École Polytechnique Fédérale de Lausanne, 1015 Lausanne, Switzerland (M.A.M.).

Notes

The authors declare no competing financial interest.

■ ACKNOWLEDGMENTS

This work was supported by the Assistant Secretary for Energy Efficiency and Renewable Energy, Fuel Cell Technologies Office, of the U.S. Department of Energy under Contract No. DE-AC02-05CH11231. Analytical TEM and portions of the cryo TEM studies were performed at the Molecular Foundry, and the SAXS experiments were performed at the Advanced Light Source (ALS) Beamline 7.3.3, both of which are supported by the Office of Science, Office of Basic Energy Sciences, Scientific User Facilities Division, of the U.S. Department of Energy under Contract No. DE-AC02-05CH11231. A.M.M. acknowledges support from the Electron Microscopy of Soft Matter Program supported by the Director, Office of Science, Office of Basic Energy Sciences, Materials Science and Engineering Division, of the U.S. Department of Energy under Contract No. DE-AC02-05CH11231. The authors thank Karen Bustillo for assistance with the XEDS measurements, and Arun Persaud, Alexander Hexemer, and Singanallur Venkatakrishnan for valuable discussions.

■ REFERENCES

- (1) Mauritz, K. A.; Moore, R. B. *Chem. Rev.* **2004**, *104*, 4535–85.
- (2) Hickner, M. A.; Pivovar, B. S. *Fuel Cells* **2005**, *5*, 213–229.
- (3) Smitha, B.; Sridhar, S.; Khan, A. A. *J. Membr. Sci.* **2005**, *259*, 10–26.
- (4) Hamrock, S. J.; Yandrasits, M. A. *J. Macromol. Sci., Part C: Polym. Rev.* **2006**, *46*, 219–244.
- (5) Gierke, T. D.; Munn, G. E.; Wilson, F. C. *J. Polym. Sci., Polym. Phys. Ed.* **1981**, *19*, 1687–1704.
- (6) Gebel, G. *Polymer* **2000**, *41*, 5829–5838.
- (7) Gebel, G.; Diat, O. *Fuel Cells* **2005**, *5*, 261–276.
- (8) Schmidt-Rohr, K.; Chen, Q. *Nat. Mater.* **2008**, *7*, 75–83.
- (9) Kreuer, K. D.; Portale, G. *Adv. Funct. Mater.* **2013**, *23*, 5390–5397.
- (10) Rubatat, L.; Rollet, A. L.; Gebel, G.; Diat, O. *Macromolecules* **2002**, *35*, 4050–4055.
- (11) Elliott, J. A.; Wu, D.; Paddison, S. J.; Moore, R. B. *Soft Matter* **2011**, *7*, 6820–6827.
- (12) Haubold, H.-G.; Vad, T.; Jungbluth, H.; Hiller, P. *Electrochim. Acta* **2001**, *46*, 1559–1563.
- (13) Kusoglu, A.; Savagatrup, S.; Clark, K. T.; Weber, A. Z. *Macromolecules* **2012**, *45*, 7467–7476.
- (14) Modestino, M. A.; Paul, D. K.; Dishari, S.; Petrina, S. A.; Allen, F. I.; Hickner, M. A.; Karan, K.; Segalman, R. A.; Weber, A. Z. *Macromolecules* **2013**, *46*, 867–873.
- (15) Kusoglu, A.; Kushner, D.; Paul, D. K.; Karan, K.; Hickner, M. A.; Weber, A. Z. *Adv. Funct. Mater.* **2014**, *24*, 4763–4774.
- (16) Kreuer, K. D.; Paddison, S. J.; Spohr, E.; Schuster, M. *Chem. Rev.* **2004**, *104*, 4637–4678.
- (17) Kong, X.; Schmidt-Rohr, K. *Polymer* **2011**, *52*, 1971–1974.
- (18) He, Q.; Kusoglu, A.; Lucas, I. T.; Clark, K.; Weber, A. Z.; Kostecki, R. J. *Phys. Chem. B* **2011**, *115*, 11650–11657.
- (19) Bass, M.; Berman, A.; Singh, A.; Kononov, O.; Freger, V. J. *Phys. Chem. B* **2010**, *114*, 3784–3790.
- (20) Ceynowa, J. *Polymer* **1978**, *19*, 73–76.
- (21) Fujimura, M.; Hashimoto, T.; Kawai, H. *Macromolecules* **1982**, *15*, 136–144.
- (22) Xue, T.; Trent, J. S.; Osseo-Asare, K. *J. Membr. Sci.* **1989**, *45*, 261–271.
- (23) Porat, Z.; Fryer, J. R.; Huxham, M.; Rubinstein, I. *J. Phys. Chem.* **1995**, *99*, 4667–4671.
- (24) Yakovlev, S.; Balsara, N. P.; Downing, K. H. *Membranes* **2013**, *3*, 424–439.
- (25) Wang, C.; Krishnan, V.; Wu, D.; Bledsoe, R.; Paddison, S. J.; Duscher, G. *J. Mater. Chem. A* **2013**, *1*, 938–944.
- (26) Rubatat, L.; Gebel, G.; Diat, O. *Macromolecules* **2004**, *37*, 7772–7783.
- (27) Modestino, M. A.; Kusoglu, A.; Hexemer, A.; Weber, A. Z.; Segalman, R. A. *Macromolecules* **2012**, *45*, 4681–4688.
- (28) Eastman, S. A.; Kim, S.; Page, K. A.; Rowe, B. W.; Kang, S.; Soles, C. L.; Yager, K. G. *Macromolecules* **2012**, *45*, 7920–7930.
- (29) Allen, F. I.; Watanabe, M.; Lee, Z.; Balsara, N. P.; Minor, A. M. *Ultramicroscopy* **2011**, *111*, 239–244.
- (30) Watanabe, M.; Allen, F. I. *Ultramicroscopy* **2012**, *113*, 106–119.
- (31) Agulleiro, J. I.; Fernandez, J. J. *Bioinformatics* **2011**, *27*, 582–583.
- (32) Feng, S.; Voth, G. A. *J. Phys. Chem. B* **2011**, *115*, 5903–5912.
- (33) Gavish, N.; Jones, J.; Xu, Z.; Christlieb, A.; Promislow, K. *Polymers* **2012**, *4*, 630–655.
- (34) Elliott, J. A.; Paddison, S. J. *Phys. Chem. Chem. Phys.* **2007**, *9*, 2602–2618.
- (35) Schmidt-Rohr, K. *J. Appl. Crystallogr.* **2007**, *40*, 16–25.